JOURNAL OF MATERIALS SCIENCE 28 (1993) 5580–5591

Fatigue behaviour of borosilicate glass–ceramic matrix, nicalon (silicon carbide) fibre composites

V. RAMAKRISHNAN, N. JAYARAMAN
Department of Materials Science and Engineering, University of Cincinnati, Cincinnati, OH 45221-0012, USA

Uniaxial fatigue damage analyses were performed on borosilicate glass–ceramic matrix, Nicalon (silicon carbide) fibre reinforced unidirectional composites. The fibre volume fraction varied from about 0.25 to 0.60. Load-controlled tension–tension fatigue tests (R ratio = 0.1) were conducted at room temperature and 540 °C (1000 °F). The fatigue life was found to decrease with increasing cyclic stress level and a power-law relationship of the form $\sigma_{app} = \sigma_{uts}(2N_f)^b$ was established where σ_{app} is the applied maximum stress, σ_{uts} the monotonic tensile strength, N_f is the number of cycles to failure and b is the fatigue strength exponent. The fatigue damage evolution manifested itself as a decrease in stiffness of the composite with fatigue cycles. This stiffness drop was associated with matrix cracking followed by fibre–matrix debonding and fibre sliding breakage/pull-out, and final failure, respectively at 540 °C. The damage evolution at room temperature was associated with degradation of the matrix followed by steady breakage of fibres with no debonding/pull-out, leading to eventual failure of the net section of the composite. In general, quantitative microscopic observations of debonded and pulled-out fibres showed a good correlation with the observed reduction in stiffness. A predictive model to interpret the drop in stiffness is presented and validated using experimental results from the current study.

1. Introduction

The increasing need for high-performance materials has generated a great deal of interest in glass and glass–ceramic matrix composites reinforced with ceramic fibres. They have been found to possess high strength, high stiffness, excellent toughness and low density [1, 2]. Lithium aluminium silicate (LAS) glass and borosilicate glass matrix composites have been extensively studied [3–9]. LAS glasses generally have higher service temperature capabilities and exhibit higher strength levels [5].

Borosilicate glass matrices reinforced with Nicalon (silicon carbide) type yarn provide a good model system due to excellent compatibility between the fibre and matrix. For example, borosilicate glass and Nicalon fibres have similar coefficients of thermal expansion (3.25×10^{-6} and $4.0 \times 10^{-6}\,°C^{-1}$, respectively) [1, 2], which should result in minimum residual stresses on fabrication. Another attractive feature is the relative ease of processing due to the unique capability of glasses to be densified in the glassy state and then crystallized by controlling the processing temperatures. The availability of silicon carbide in the form of yarn, i.e. Nicalon, makes it easier to incorporate it as a reinforcement in the composite.

For the efficient use of materials in any application, the failure mechanisms and damage behaviour under static and dynamic conditions must be well understood. Initial studies on mechanical behaviour (tensile, fatigue, etc.,) of ceramic matrix composites were based on three-point and four-point bend tests, but more recent studies in the literature were found to be based on uniaxial tension tests [3–9]. Prewo and co-workers [1–5, 7] found that if the composite (LAS matrix) was cycled at a stress less than 65% of its ultimate (flexural or tensile) strength or below the "proportional limit", it survived an arbitrarily set limit of 100 000 cycles with no significant loss of stiffness or strength, while stiffness was found to decrease with cycling if the cyclic stress was above the proportional limit.

The present work attempts to understand the fatigue damage evolution process by making correlations between observed microstructural damage and properties in composites of borosilicate glass–ceramic matrix reinforced with Nicalon fibres. An earlier paper described the mechanical behaviour of this material under conditions of monotonic tension at temperatures ranging from room temperature to 650 °C [10].

2. Experimental procedure

2.1 Composite fabrication

The basic process used for the manufacture of these composites was developed at the United Technologies Research Center by Prewo *et al.* [1, 2]. The process

0022–2461

followed in the current research programme consisted of several steps. After desizing, the tows of fibres of Nicalon were passed through a slurry containing glass frit (325 mesh) of Corning 7740 (borosilicate glass) with a binder (Robond) and wound on a hexagonal drum. After drying, these pre-pregs were stacked to give eight unidirectional plies, and the binder was burned out by heating the plies to 500 °C for 0.5 h, and hot-pressed at 1000 °C under a pressure of 1000 psi (6.9 MPa) for 15 min in a graphite die using graphite punches. This was followed by furnace-cooling in argon and under pressure. The pressure was removed once the softening point (821 °C) was passed. Plates containing fibre volume fractions from 0.25 to 0.6 were thus manufactured for monotonic and fatigue testing.

2.2. Composite characterization

Microstructural analyses by optical microscopy and SEM reveal the composite to be made of fibre-rich regions in the plies along with matrix-dominated inter-ply regions in the lower-V_f composites (Fig. 1a and b). Fig. 2 shows a schematic diagram of the structure of the composite. Phase analyses by X-ray diffraction revealed the matrix in the inter-ply region to be essentially composed of the alpha (low) cristobalite polymorph of SiO_2. There are also thick grain boundary-like features around the alpha cristobalite crystals which appear to be fully glass. The matrix in the ply region appears to be fully glass with a composition close to Corning 7740 borosilicate glass. Details of the characterization studies are discussed in an earlier publication [3].

2.3. Test procedures

Straight strip specimens of length 12.7 cm, width 0.64 cm and thickness 0.25 cm were cut off the composite plate using a diamond blade with a low-speed saw. All tests were conducted on a closed-loop servo-hydraulic testing machine, using a set of water-cooled mechanical wedge grips. Tapered stainless steel end-tabs were used in the grip area of the specimens. The samples were indirectly heated using an induction-heated stainless steel susceptor. A high-temperature MTS extensometer (gauge length = 20 mm) with alumina rods was used for the monitoring strain.

Monotonic tension tests were performed at temperatures [10] ranging from room temperature to 650 °C. All tests were performed under load control (load rate = 12.4 $N s^{-1}$) and a few additional tests were performed under stroke control (strain rate = 4×10^{-5} s^{-1}).

Load-control fatigue tests were performed with a sinusoidal waveform at a frequency of 0.33 Hz, R-ratio of 0.1, at room temperature and 540 °C. Load, strain, stroke and time data were collected and stored in a PC throughout the test. These data were used to monitor the strain and the modulus (stiffness) during fatigue tests. Fatigue damage analyses were done by microstructural examination of longitudinal and transverse cross-sections of the tested specimens. Quantitative

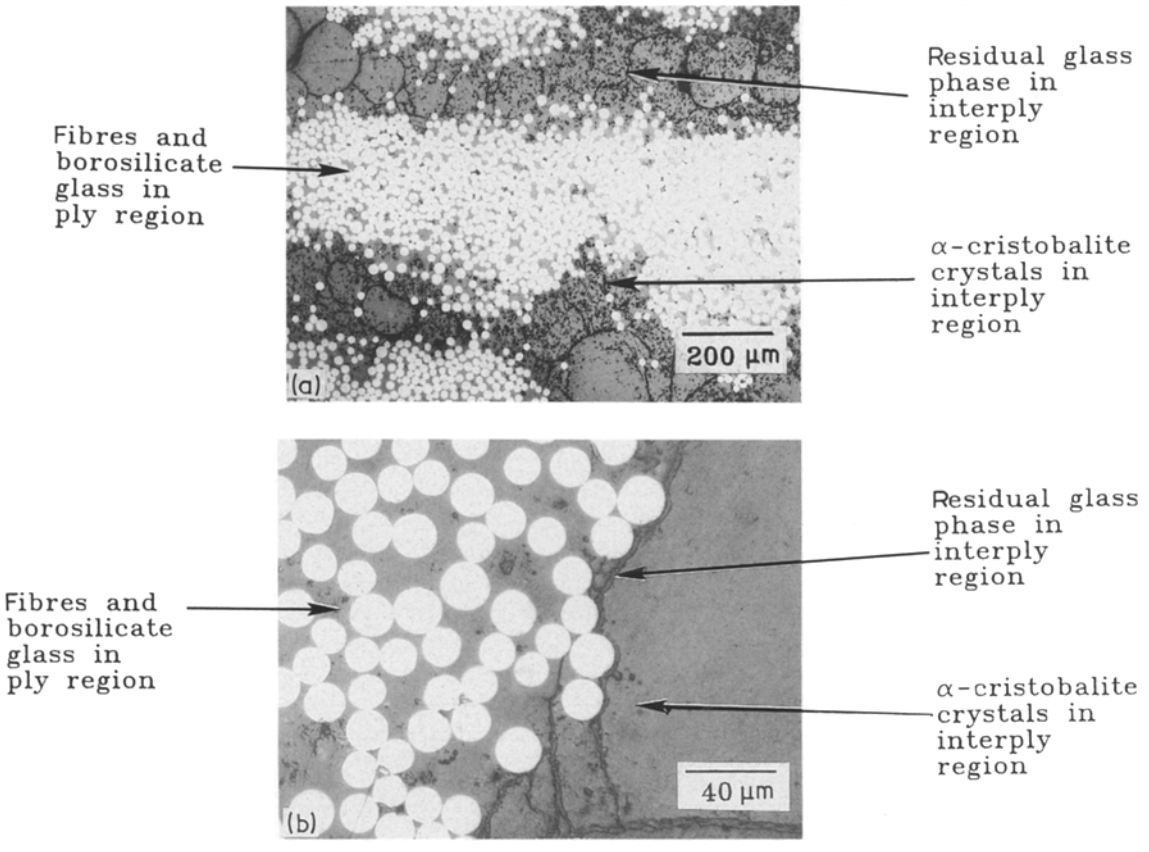

Figure 1 (a, b) Microstructure of as-processed composite; $V_f = 0.35$.

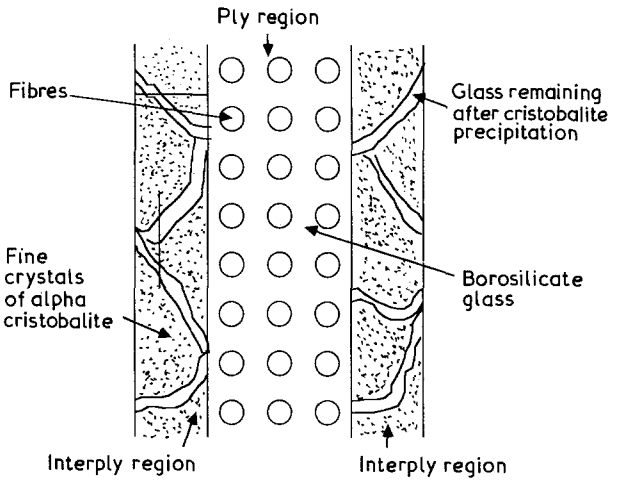

Figure 2 Schematic diagram showing structure of the composite.

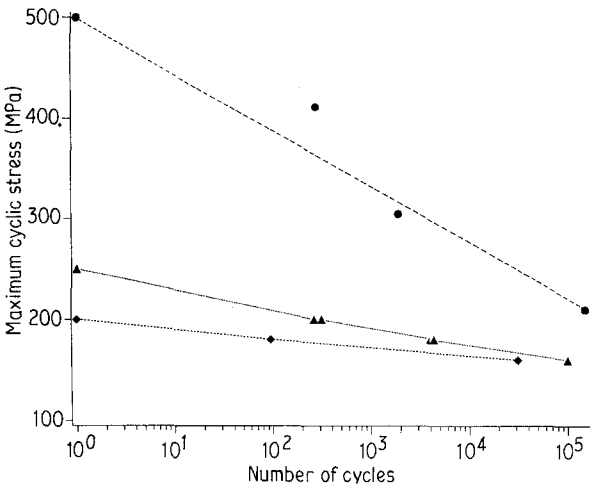

Figure 3 Stress versus number of cycles for various conditions: (●) 540 °C, V_f = 0.5–0.6; (▲) 540 °C, V_f = 0.35–0.5; (◆) R.T., V_f = 0.25–0.35.

analyses of debonded fibres and broken fibres were conducted and correlated with changes in strain and modulus.

3. Results

3.1. Monotonic tensile behaviour

Important observations on the monotonic tensile behaviour of these glass–ceramic composites are listed below and more detailed descriptions may be obtained from our previous paper [10].

1. Room-temperature tensile strength was around 200 MPa and it was unaffected by temperature up to about 425 °C. The strength increases dramatically to about 300 MPa at 540 °C followed by a decrease at higher temperatures. This increase in strength was attributed to the strain point of Corning 7740 borosilicate glass.

2. The modulus of elasticity (stiffness) was found to decrease with temperature from about 100 GPa at room temperature to about 85 GPa at 540 °C.

3. The general monotonic tensile failures were attributed to matrix cracking and longitudinal splitting at room temperature and fibre failure and pull-out at higher temperatures.

3.2. Fatigue behaviour

Table I summarizes the fatigue test results obtained under different conditions of test temperature and cyclic stress level. Fig. 3 shows the plot of stress versus number of cycles to failure. A power-law correlation between the cyclic stress and fatigue life was observed. The corresponding life equations are of the form

$$\sigma_{app} = \sigma_{uts}(2N_f)^b$$

where σ_{app} = applied maximum stress, $2N_f$ = number of reversals to failure (1 cycle = 2 reversals), σ_{uts} = monotonic tensile strength, and b = fatigue strength exponent (similar to the Coffin–Manson exponent). The actual values obtained for σ_{uts} and b are

TABLE I Summary of fatigue test results

Specimen/batch[a]	V_f[b]	$E_{c,init}$ (GPa)[c]	Temp (°C)	Stress level (MPa)	N_f
4A[d]/A	0.55	109	540	210	⩾ 150 000
4B/A	0.51	99	540	412	277
4C/A	0.60	117	540	305	1900
20-3[d]/B	0.50	109	540	160	⩾ 100 000
32-5/B	0.35	80.5	540	180	3982
20-2[e]/B	0.50	–	540	180	4350
20-5/B	0.50	122.5	540	200	302
32-4/B	0.35	85.5	540	200	316
42-1/B	0.42	93	540	200	265
34-6/B	0.30	86	R.T.	180	95
34-8/B	0.24	77	R.T.	160	31276

[a] The plates made from Batch A exhibited higher strength for similar volume fractions of fibres compared to Batch B. It is believed that while the strength is affected due to microstructural differences (such as amount and distribution of α-cristobalite in the matrix) between the two batches of samples, the initial stiffness ($E_{c,init}$) is not significantly affected.
[b] V_f is the actual volume fraction of fibres in the tested specimen, measured by quantitative metallography techniques.
[c] $E_{c,init}$ is the stiffness measured in the first cycle.
[d] No stiffness drop observed.
[e] Stiffness data not recorded. Life data used for power-law correlation.

TABLE II Constants from power-law correlation

Temperature	V_f	σ_{uts}(MPa)[a]	b
540 °C	0.50–0.60	500	– 0.0705
540 °C	0.35–0.50	250	– 0.0388
R.T.	0.25–0.30	200	– 0.0205

[a] σ_{uts} values reported here are from the power-law stress-life equation. At 540 °C, the actual σ_{uts} determined through monotonic tensile tests differed slightly from these values, which was attributed to strain-rate differences between the tensile and fatigue tests [10].

listed in Table II. This type of power-law correlation has been observed for other brittle matrix composite systems, for example, Hwang and Han [11] found a similar correlation for the glass–epoxy system.

Load, strain and actuator displacement (stroke) values were collected as a function of time for all cycles in all tests. In a load-controlled test, strain (or stroke) response versus cycles will help understand the evolution of constitutive behaviour during fatigue cycles. Fig. 4, a typical plot of the strain versus time, shows that the strain range increases with cycling. The rate of increase of strain range generally depended on the temperature and cyclic stress level of testing. Thus, the stiffness was found to decrease with cycles. For lower cyclic stresses, no significant drop in stiffness was found.

In composite materials, due to the inherent inhomogeneity, the strain is distributed non-uniformly in the material. This non-uniform distribution could lead to somewhat erroneous results when measured by conventional extensometry, due to the strain measured by the extensometer being local as opposed to that measured by the stroke data which is global. This leads to the following two observations:

(i) The strain measured by conventional extensometers tends to show more variations due to local damage (such as sudden strain drop), while the strain measured using the actuator displacement (i.e. stroke data) gives the average strain. Fig. 5 a and b show a typical example illustrating this point. Here, the stroke (i.e. actuator displacement) data were converted to strain after appropriately subtracting the displacement due to the compliance of the machine. This procedure was first validated by conducting a similar analysis using specimens of monolithic 1040 steel in which the extensometer measurements correlated well with the actuator stroke measurements.

(ii) The reduction in stiffness during fatigue calculated using strain values from a conventional extensometer is always smaller than that using strain values from stroke data (after correcting for machine compliance). Fig. 6 shows a plot of stiffness versus cycles for Specimen 32-4 (Table I) as calculated from extensometer and stroke data. We see that while both the curves overlap initially, as the cycling progresses the stroke curve steadily deviates downward from the extensometer curve, implying that the entire composite has undergone greater damage than that indicated by the extensometer. This was observed for all the specimens tested. In fact, this behaviour was also observed in monotonic tensile tests where the stress–strain curve calculated from stroke data steadily deviated from the stress–strain curve calculated from extensometer data, even though they overlap well in the initial stages.

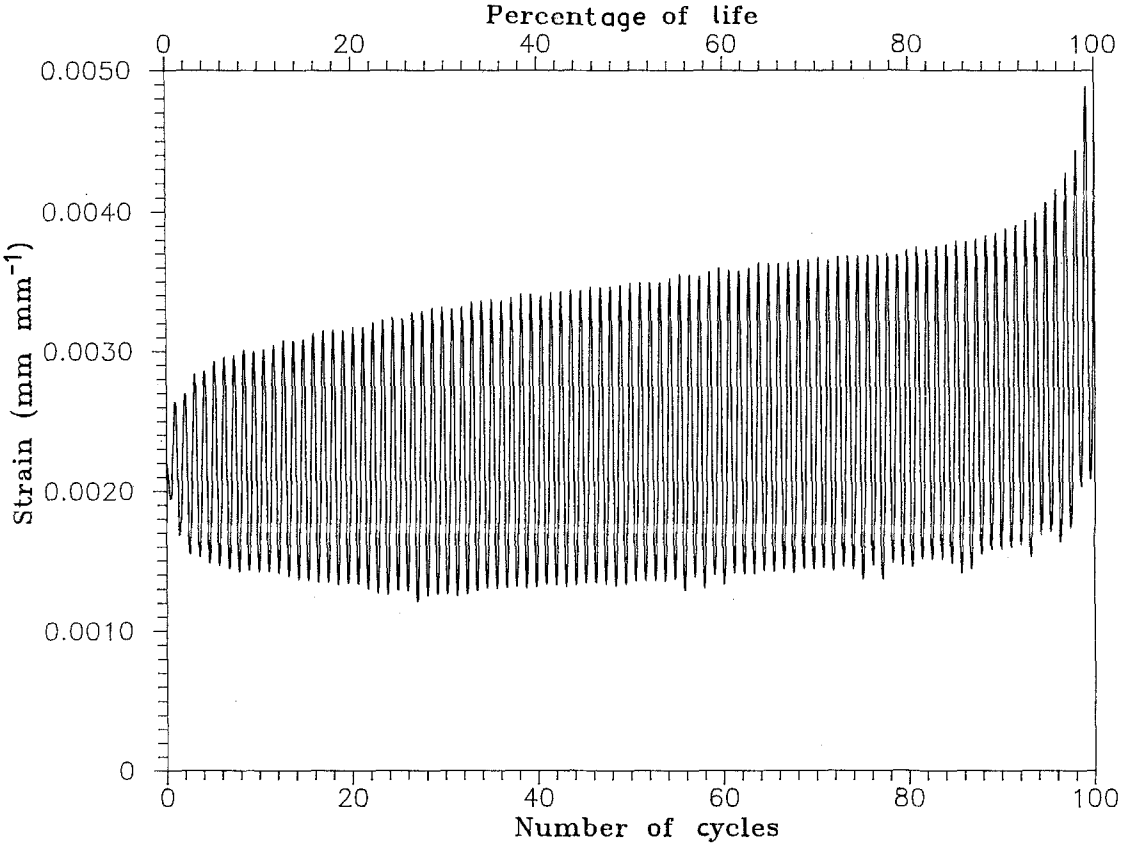

Figure 4 Strain versus number of cycles/percentage of life for specimen 34-6 (Table I) showing increasing strain with cycling.

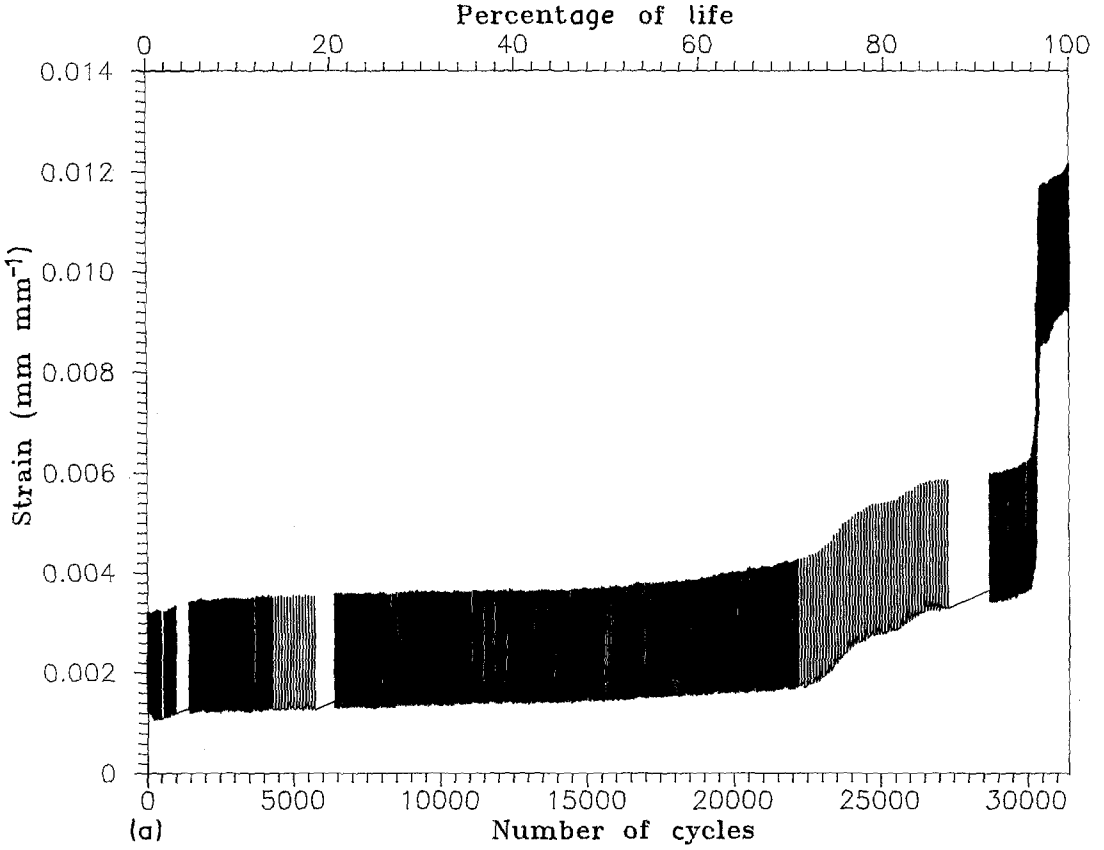

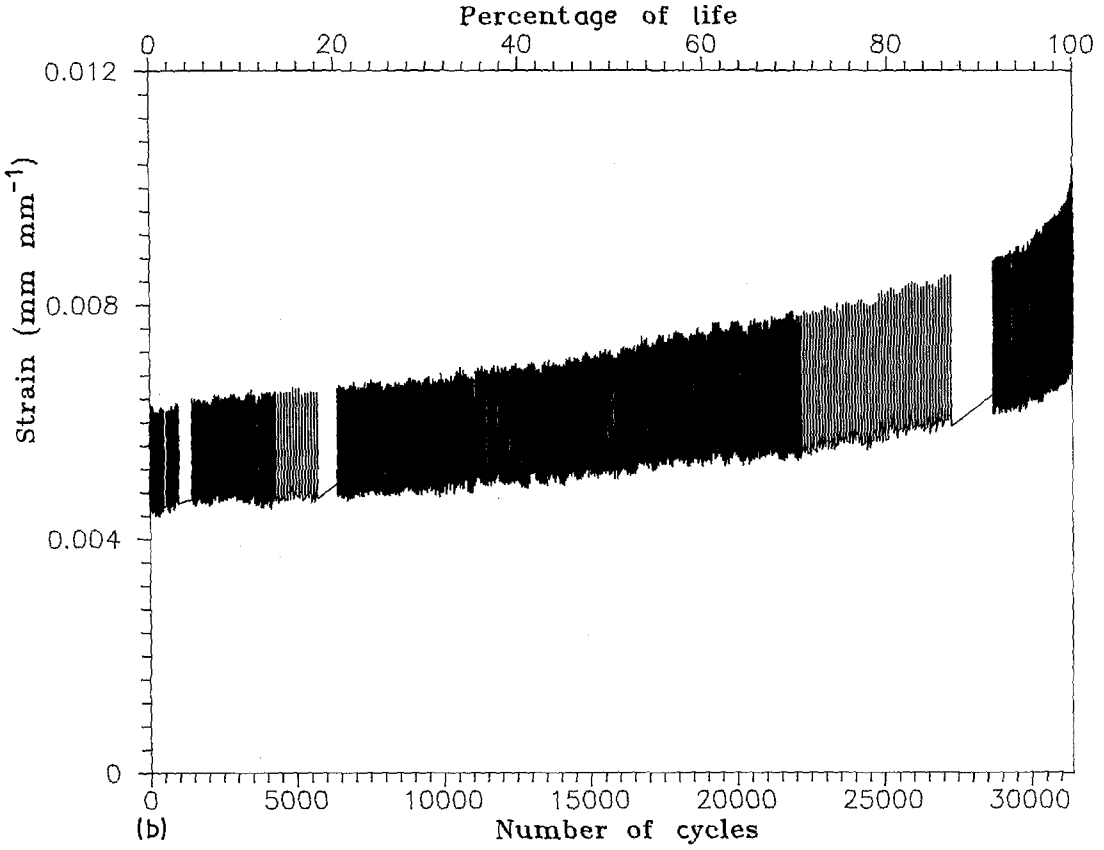

Figure 5 (a) Strain (from extensometer) versus number of cycles/percentage of life for specimen 34-8 (Table I) showing abrupt local variations in strain; (b) : Strain (from stroke) for same specimen showing smoother variations in strain.

It is therefore obvious that all damage analysis must be conducted on the stiffness drop curves obtained from global strain measurements, if the damage is to be calculated from composite constituent properties, e.g. V_f and V_m. Ideally, this should be done using strain measuring devices that can measure the total displacement in the entire composite specimen. In this research, the global strain measurements were made using the actuator displacements (stroke) after appropriately subtracting displacements due to machine

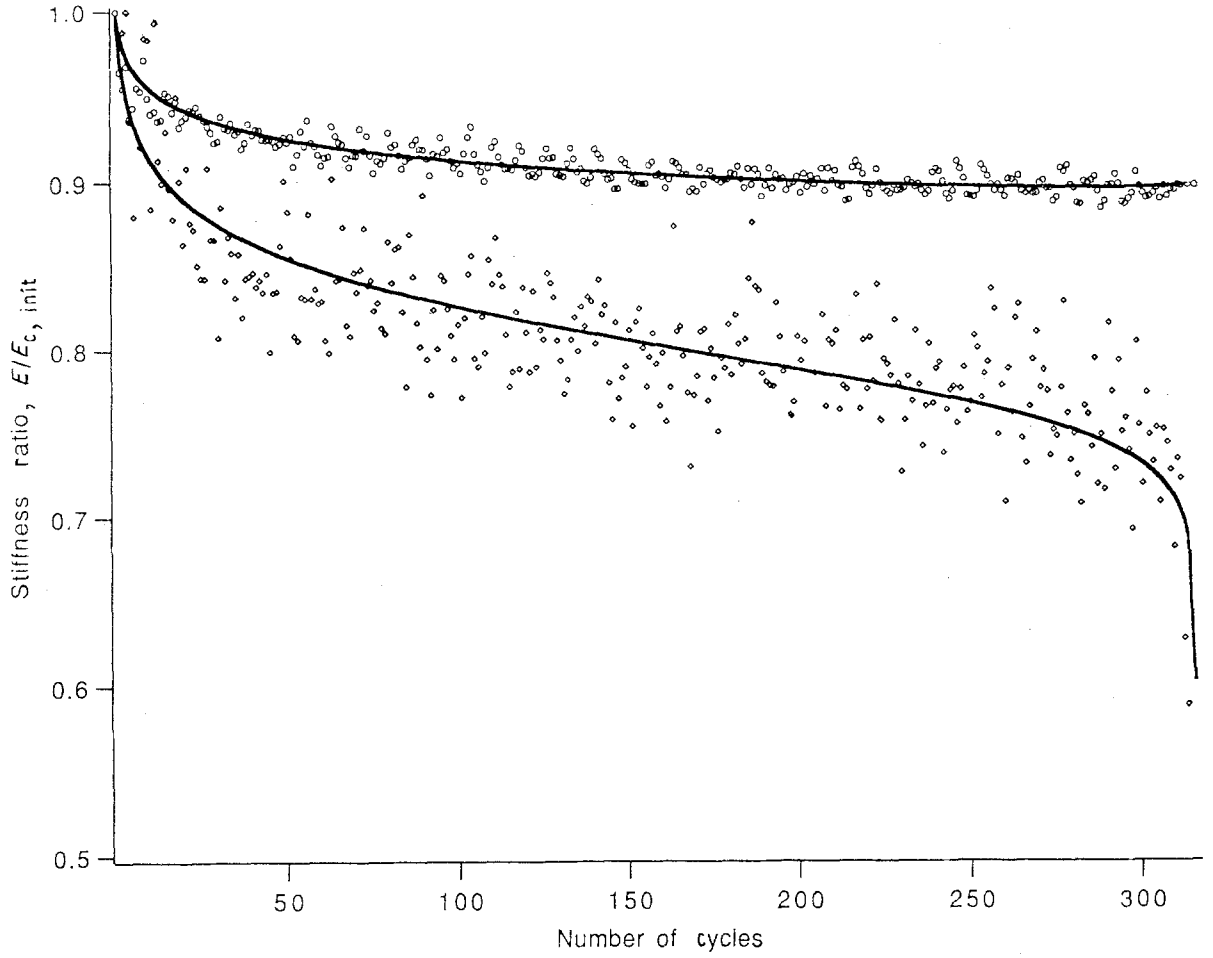

Figure 6 Plot of stiffness versus number of cycles for specimen 32-4 (Table I) showing differences in damage as measured by the two methods: (o) strain data, (◇) stroke data.

compliance. These measurements were later found to be very useful in developing a mechanistically based damage evolution model [12].

3.3. Microstructural analysis

Microstructural analysis was done to develop a physical understanding of the process of damage evolution during fatigue. Fig. 7a and b show the unetched microstructures of transverse cross-sections of specimens that were subjected to fatigue at room temperature and 540 °C, respectively. Fig. 7a is the microstructure of the sample subjected to room-temperature fatigue. We can see significant fibre damage (broken and pulled-out fibres) within the ply regions. Observations at higher magnifications did not reveal any significant debonding between the matrix and fibre. In contrast, Fig. 7b, for the high-temperature fatigue cycled condition, shows most of the fibres being intact except for localized regions from where fibres seem to have pulled out. On careful examination of the microstructure at higher magnifications, several instances of debonding at the fibre–matrix interface were discovered. A magnified view illustrating this is shown in Fig. 8. Longitudinal sections confirmed that fibre–matrix debonding has occurred in several regions.

To quantify the observed damage mechanisms, photomicrographs were taken for all samples at low

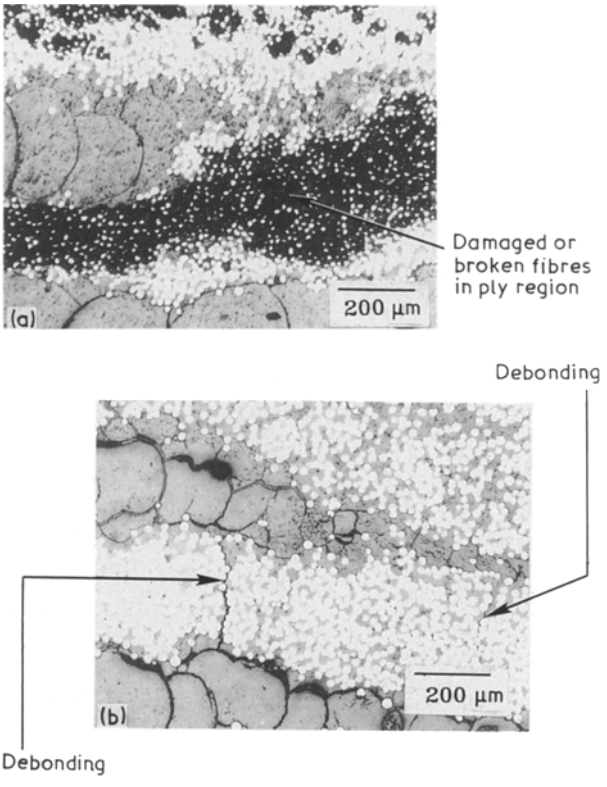

Figure 7 (a) Microstructure of specimen 34-6 (Table I) showing matrix and fibre damage; (b) Microstructure of specimen 32-5 (Table I) showing debonding, matrix cracking and some fibre damage.

TABLE III Summary of fatigue and quantitative microscopy results

Sample	Max. Stress (MPa)	Cycles to failure	Drop in stiffness (%)[a]	Metallography data	
				Debonded fibres (%)	Broken fibres (%)
20-3[b]	160	100 000	< 1	–	–
32-5	180	3982	14	8	12
33-4[b]	180	1000	40	13	37
20-5	200	303	22	17	24
32-4	200	315	11	11	15
42-1	200	263	32	7	35
34-8[c]	160	31 276	36	–	21
34-6	180	95	35	–	42

[a] Stiffness drop (%) = $[(E_{c,init} - E_{failure})/E_{c,init}] \times 100$ where $E_{failure}$ is the measured stiffness just before failure.
[b] Interrupted test.
[c] Difficulty in counting broken fibres due to vertical splitting of specimen.

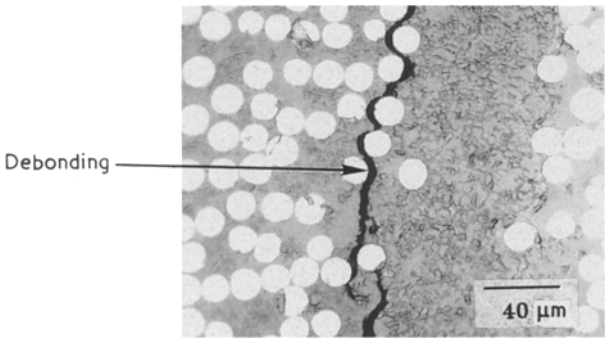

Figure 8 Magnified view of fibre–matrix debonding at 540 °C.

magnification (50 ×) and from these photomicrographs, the percentages of pulled-out or broken fibres were determined by counting them from micrographs similar to those shown in Fig. 7. The samples were then observed at a higher magnification (about 900 ×) and the number of debonded fibres was counted to get an estimation of the percentage of debonded fibres. These observations are listed in Table III and a very good correlation was made between the percentage of broken/damaged fibres and the observed stiffness drops. These observations point toward a clear picture of damage evolution during fatigue which is shown in the schematic diagram in Fig. 9. Based on the above

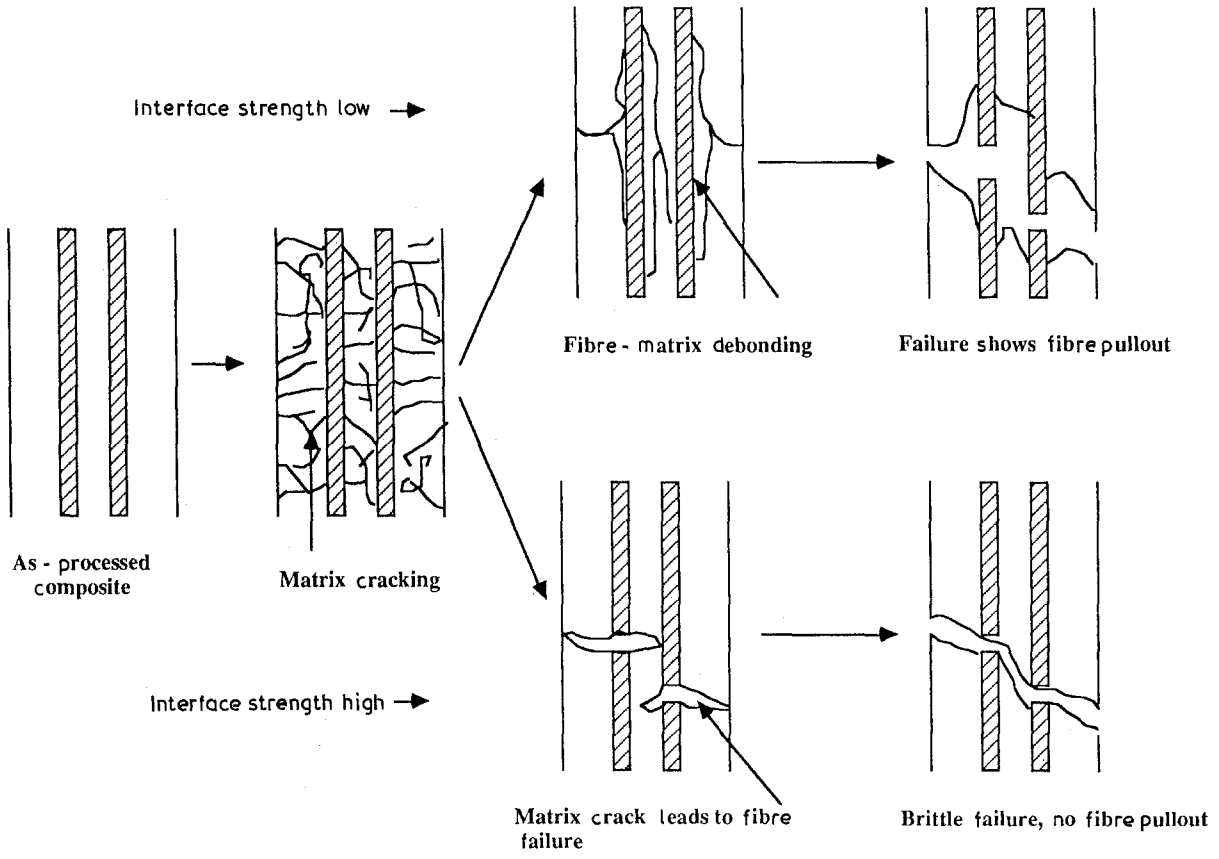

Figure 9 Schematic diagram depicting the progression of fatigue damage under different interfacial conditions.

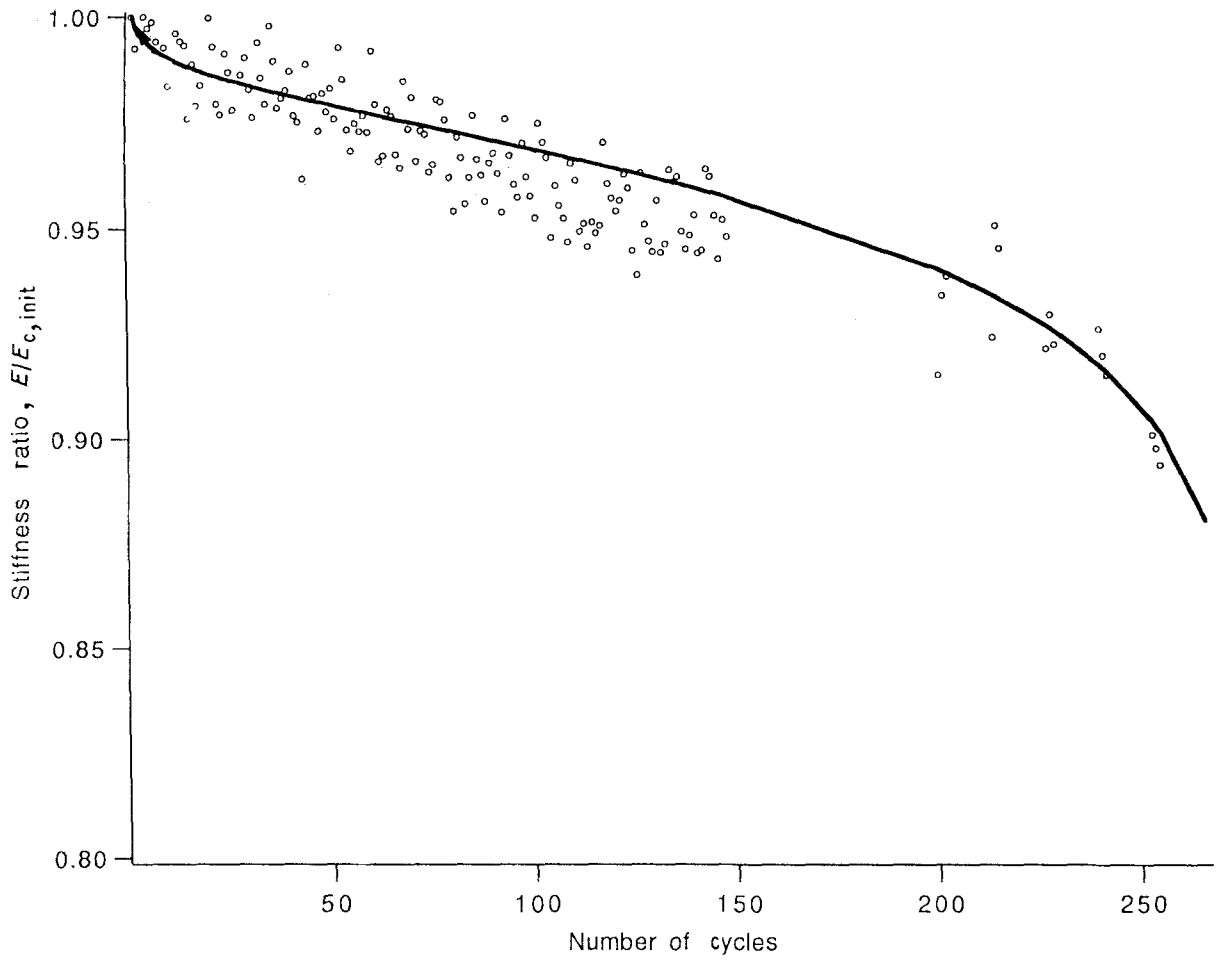

Figure 10 (——) Predicted stiffness curve for specimen 4B (Table I) with (○) experimental data superimposed.

discussion, the conditions of high interfacial strength and low interfacial strength correspond to the room temperature and 540 °C test temperatures, respectively.

4. Fatigue damage model

A model to interpret and predict fatigue damage in brittle matrix composites in general and the current composite system in particular as mentioned below is described in elsewhere [12]. This mechanistically based model uses individual contributions from the matrix and fibre stiffnesses as building blocks to calculate the cumulative damage to the composite.

The starting stiffness of any composite, ideally, under conditions of very good load transfer between the matrix and fibre, is given by the rule of mixtures, i.e.

$$E_{c,init} = E_m V_m + E_f V_f$$

or

$$1 = \frac{E_m V_m}{E_{c,init}} + \frac{E_f V_f}{E_{c,init}}$$

where $E_{c,init}$ = initial stiffness of the composite, E_m = stiffness of the matrix, E_f = stiffness of the fibre, V_m = volume fraction of matrix and V_f = volume fraction of fibres. Since the initial stiffness of the composite uses contributions from the fibre and matrix as building blocks, intuitively, any loss in stiffness of the composite must also use these two terms relating to the depletion of the stiffness of the matrix and fibre.

During the process of fatigue damage evolution, using the model developed [12] in the general case of composite systems with variable fibre–matrix interface strength, the stiffness E of the composite can be calculated after any number of cycles (from $N = 0$ to $N = N_f - 1$) using the equation

$$\frac{E}{E_c} = 1 - \frac{E_m V_m}{E_c}(1-f)\left(\frac{\ln(N+1)}{\ln N_f} + f\frac{N}{N_f}\right) + \frac{E_f V_f}{E_c}(1-r)\frac{\ln[1-(N/N_f)]}{\ln(1/N_f)} \quad (1)$$

The stiffness loss in the composite is calculated in Equation 1 by isolating the stiffness drops due to the matrix and fibre individually. Furthermore, the stiffness reduction due to matrix damage is partitioned between the two rate processes, one logarithmic, another linear. The partitioning is done through a fibre–matrix interface strength parameter, f. The interface is the least understood but the most instrumental in the determination of composite properties. As discussed elsewhere [12], f is the friction coefficient as determined by the fibre push-out test [13]. The quantity r in Equation 1 is $\sigma_{app}/\sigma_{uts}$. The significance of each of these terms is discussed in detail elsewhere [12].

Equation 1 thus represents the mechanistically based damage equation that can be used for predicting

stiffness drops as a function of cycles in a unidirectional brittle-matrix fibre-reinforced composite. All the parameters used in this equation are mechanical properties of the constituents used in the composite. Figs 10 to 16 show the predicted stiffness drop curve for specimens in Table I with the experimentally obtained data superimposed. It can be seen that in each case the agreement is excellent.

5. Conclusions

The main conclusions from this study are as follows.

1. The fatigue life was found to decrease with increasing cyclic stress level at both temperatures of testing. A power-law relationship of the form

$$\sigma_{app} = \sigma_{uts}(2N_f)^b$$

was found to exist where σ_{app} is the maximum cyclic stress, N_f, the number of cycles to failure, σ_{uts} the monotonic tensile strength and b the fatigue strength exponent, a constant.

2. In general, the strain measurements made using the extensometer were taken to be an indicator of the local damage in the composite, while the strain measured from the stroke (displacement of the actuator) were thought to be due to the overall response of the composite.

3. The total strain per stroke was found to increase and the stiffness to decrease with increasing cycling at a given stress level and temperature. The total drop in stiffness correlated well with the number of broken/damaged fibres in the composite.

4. Debonding between the fibre and matrix was observed at the higher test temperature while none was observed at room temperature, indicating a weaker bond under the former conditions and a stronger bond under the latter. Accordingly, fatigue damage was presumed to progress by matrix degradation followed by fibre failure under conditions of high interface strength, leading to an overall brittle failure. Under conditions of weakly bonded interfaces, however, debonding between the fibres and matrix was thought to follow/be concurrent with matrix degradation before fibre failure, leading to fibre pull-out and a more graceful failure.

5. A predictive model to interpret the fatigue damage in brittle-matrix composites was presented and the results validated with experimental observations from the current study.

Acknowledgement

The authors wish to acknowledge their helpful discussions with the Wright Laboratory's Material Behavior (MLLN) group, particularly the support of Dr Ted Nicholas.

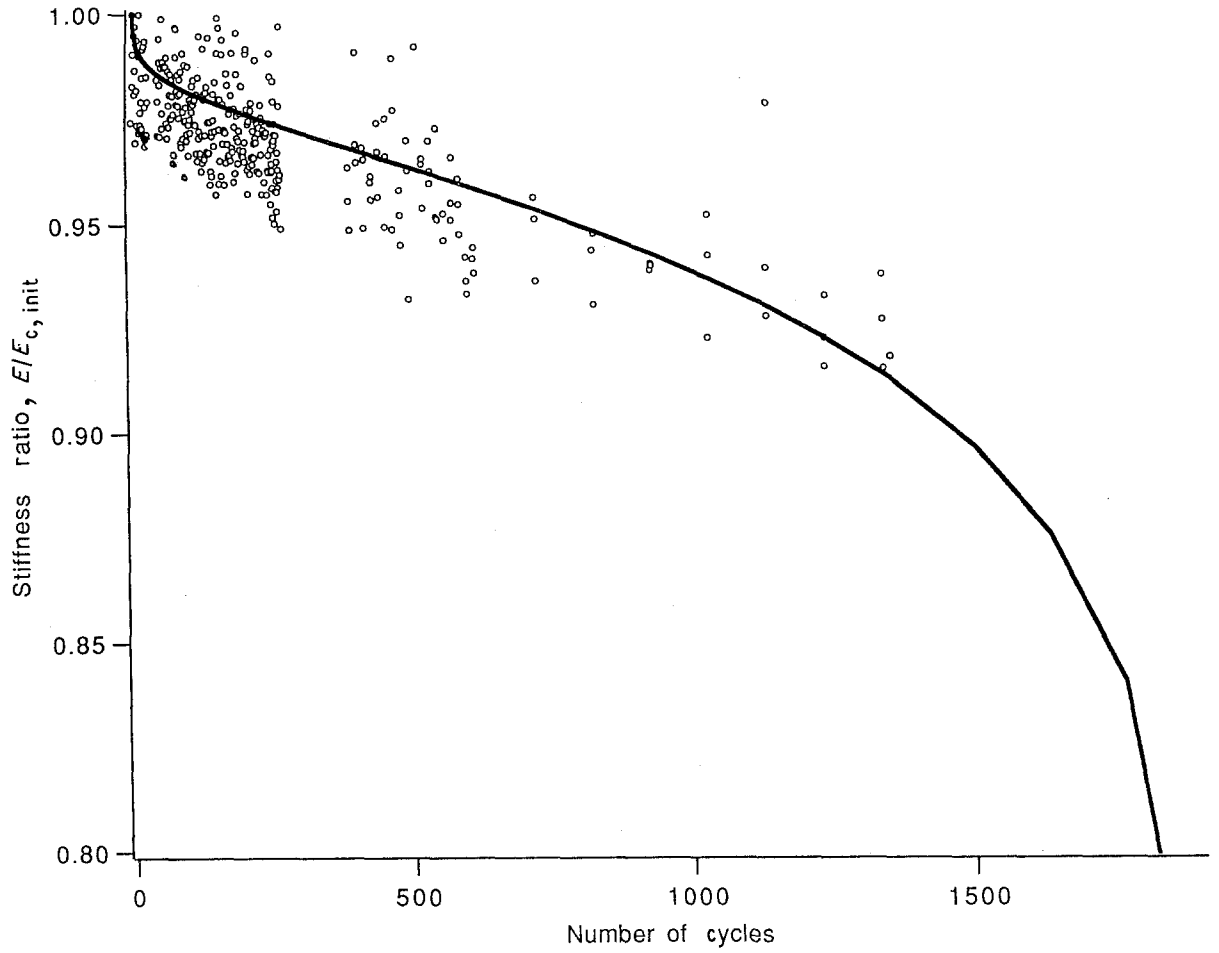

Figure 11 (——) Predicted stiffness curve for specimen 4C (Table I) with (○) experimental data superimposed.

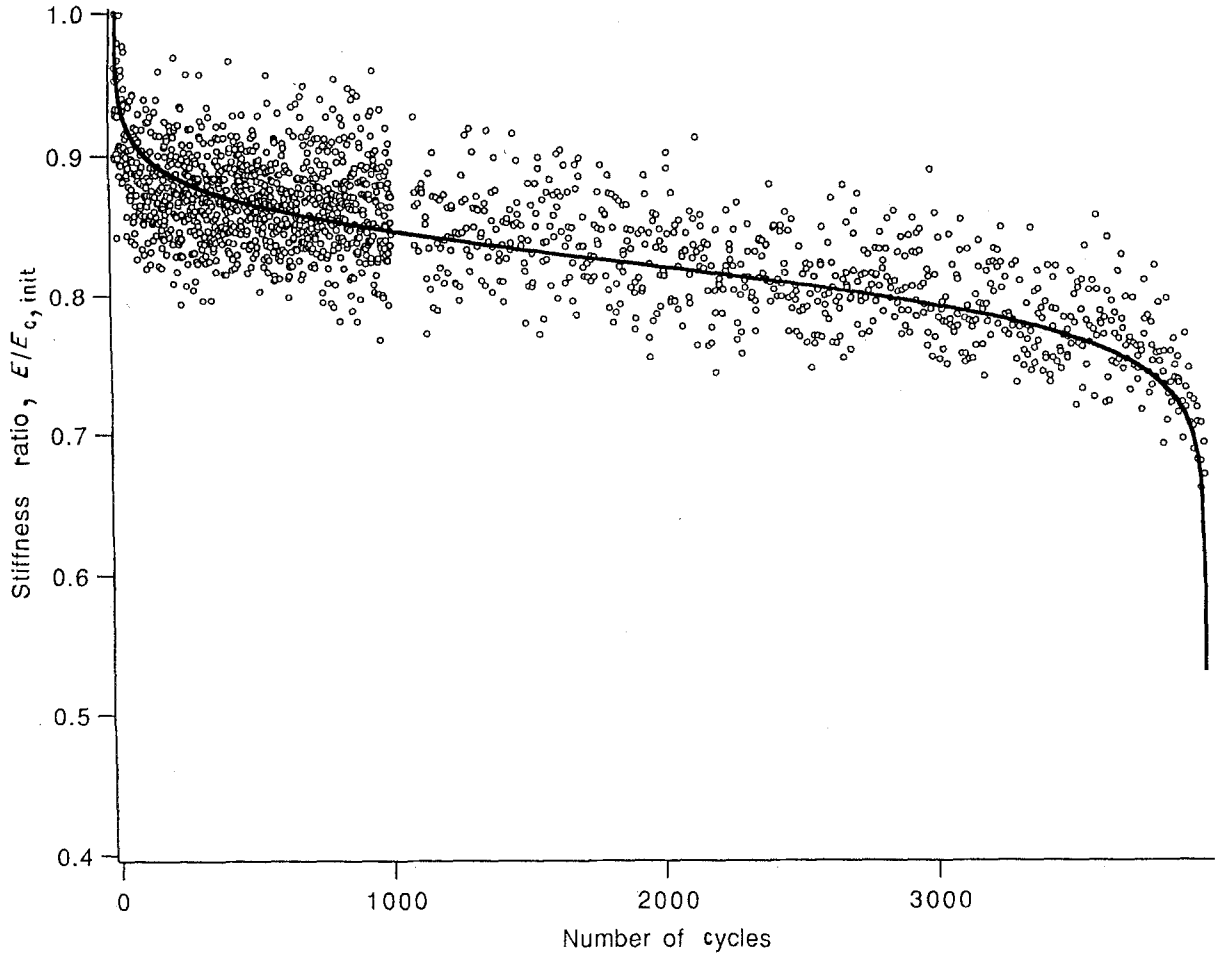

Figure 12 (——) Predicted stiffness curve for specimen 32-5 (Table I) with (○) experimental data superimposed.

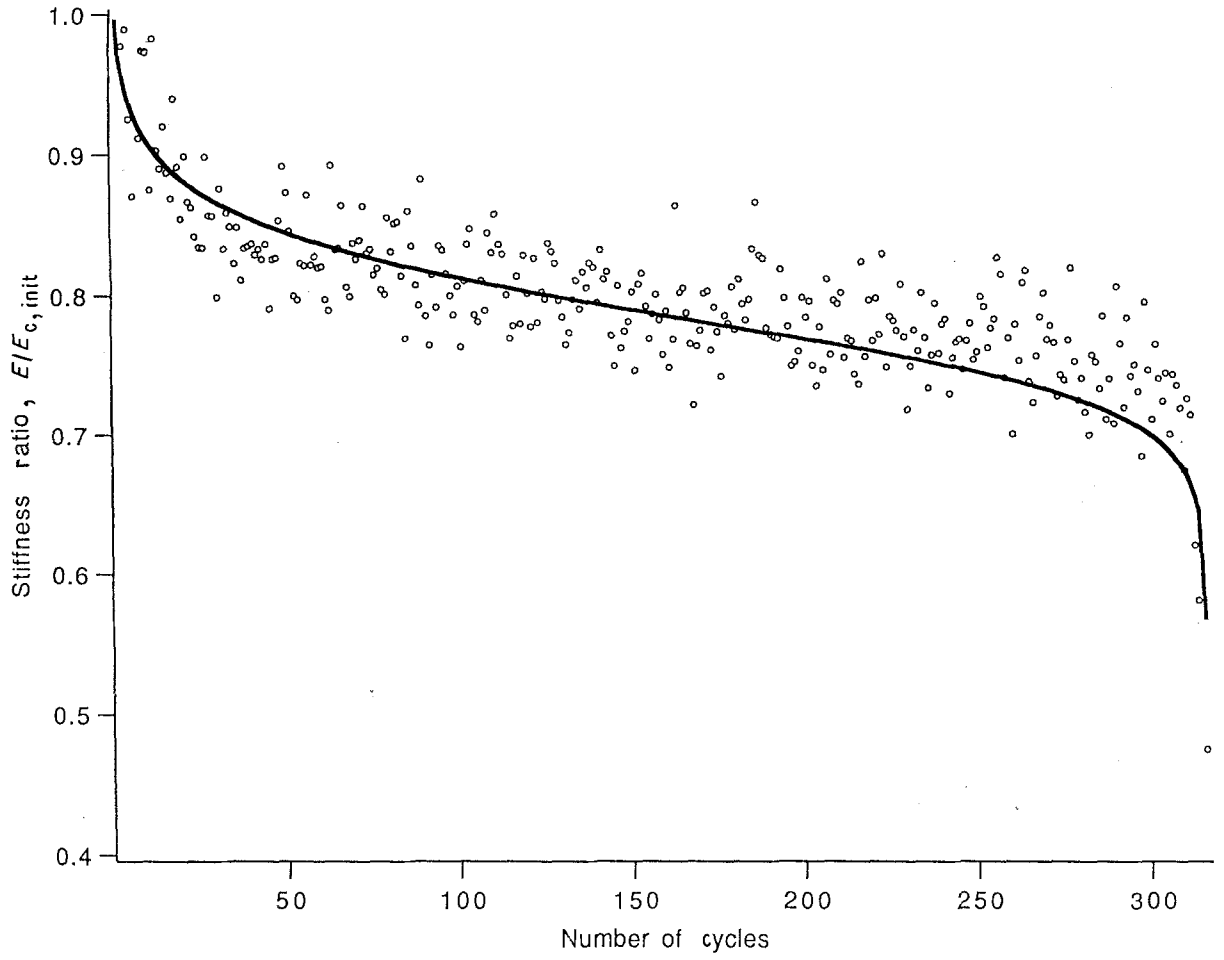

Figure 13 (——) Predicted stiffness curve for specimen 32-4 (Table I) with (○) experimental data superimposed.

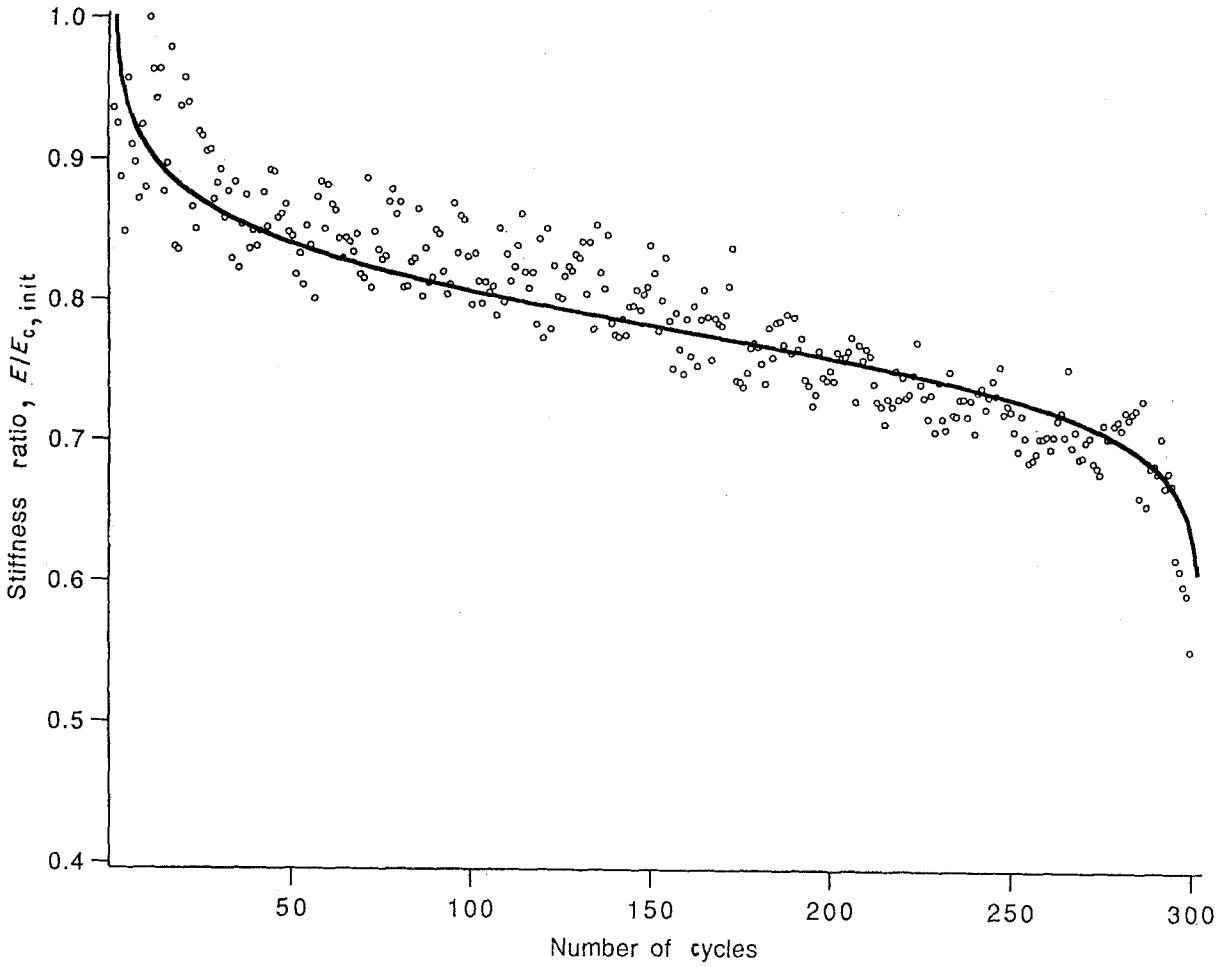

Figure 14 (——) Predicted stiffness curve for specimen 20-5 (Table I) with (○) experimental data superimposed.

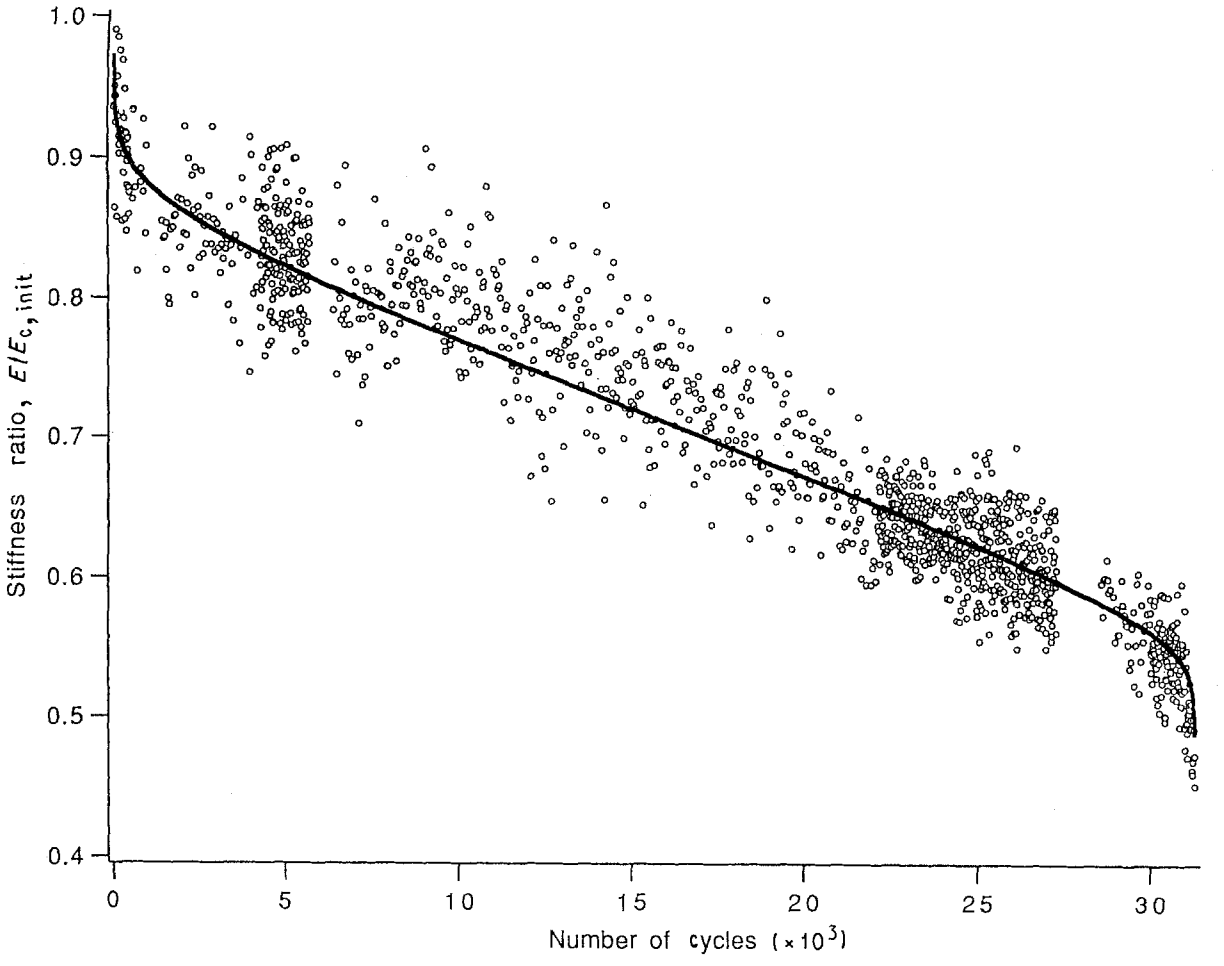

Figure 15 (——) Predicted stiffness curve for specimen 34-8 (Table I) with (○) experimental data superimposed.

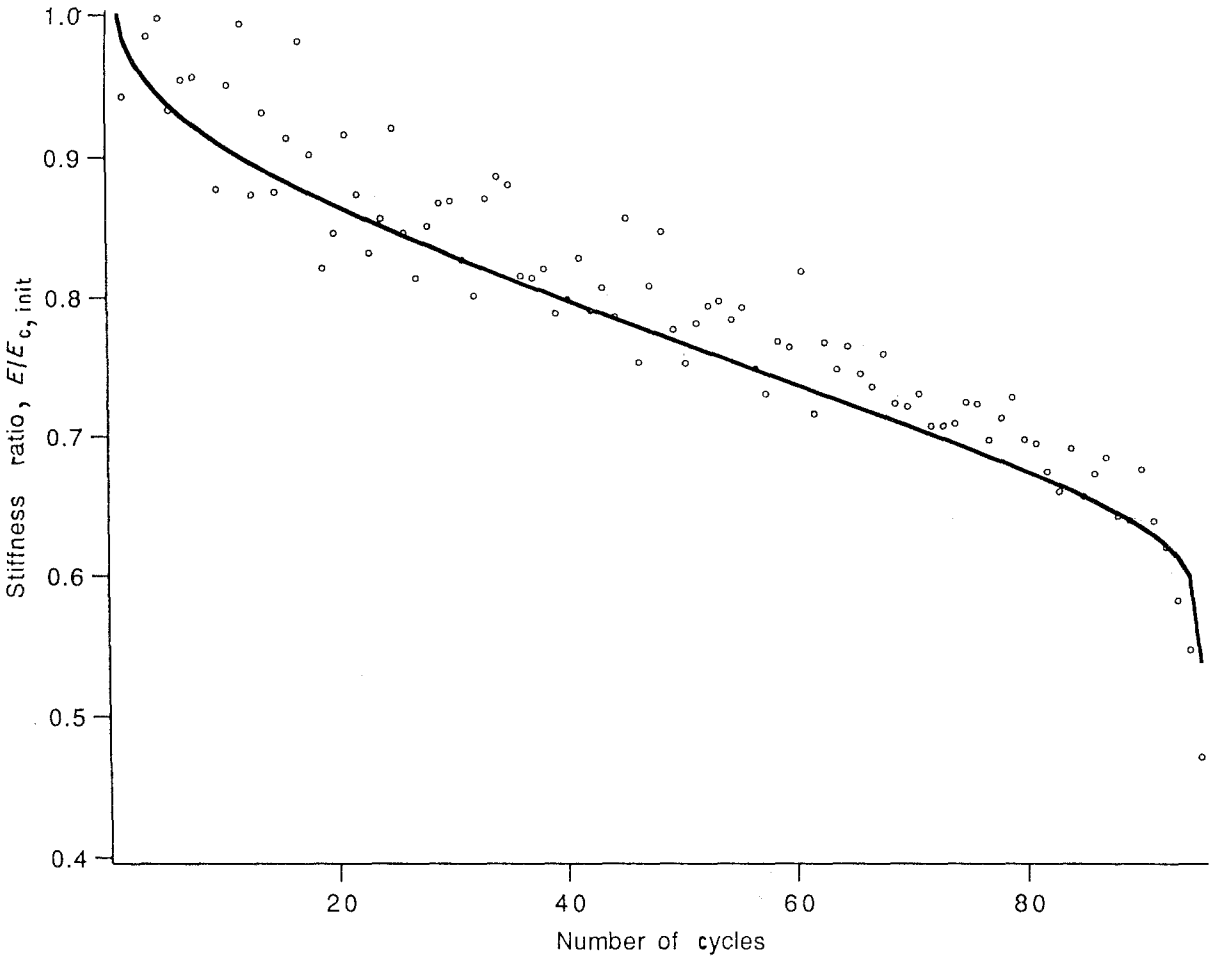

Figure 16 (——) Predicted stiffness curve for specimen 34-6 (Table I) with (○) experimental data superimposed.

References

1. K. M. PREWO, J. J. BRENNAN and G. K. LAYDEN, *Ceram. Bull.* **65** (1986) 305.
2. K. M. PREWO, *ibid.* **68** (1989) 395.
3. K. M. PREWO *et al.*, *J. Mater. Sci.* **24** (1989) 1373.
4. K. M. PREWO and J. J. BRENNAN, *ibid.* **15** (1980) 463.
5. K. M. PREWO and E. R. THOMPSON "Research on Graphite Reinforced Glass Matrix Composites", NASA CR 165711 (1981).
6. L. M. BUTKUS, L. P. ZAWADA and G. A. HARTMAN in Proceedings of Aero Mat'90, Advanced Aerospace Materials/Processes Conference, Long Beach, California, May 1990, in press.
7. K. M. PREWO, *J. Mater. Sci.* **22** (1987) 2965.
8. V. S. AVVA and J. SANKAR, "Effect of Thermal and Cyclic Loads on Silicon Carbide Yarn Reinforced Glass Matrix Composites", Final Report, DoE Contract DE-FG05-84ER45140, (1989).
9. T. KOTIL, J. W. HOLMES and M. COMNINOU, *J. Amer. Ceram. Soc.* **73** (1990) 1879.
10. V. RAMAKRISHNAN and N. JAYARAMAN, *J. Mater. Sci.* in press.
11. W. HWANG and K. S. HAN, *J. Compos. Mater.* **20** (1986) 154.
12. V. RAMAKRISHNAN and N. JAYARAMAN, submitted.
13. J. D. BRIGHT, S. DANCHAIVIJIT and D. K. SHETTY, *J. Amer. Ceram. Soc.* **74** (1991) 115.

Received 11 July 1991
and accepted 4 February 1992